ISSN 0036-0244, Russian Journal of Physical Chemistry A, 2021, Vol. 95, Suppl. 2, pp. S296–S306. © Pleiades Publishing, Ltd., 2021.

STRUCTURE OF MATTER AND QUANTUM CHEMISTRY

Predicted Structural, Elastic, Electronic, Lattice Dynamic, Thermodynamic and Optical Properties of Cubic ScF_3 from First-Principles Calculations

Mohamed Amine Ghebouli[a,*], Brahim Ghebouli[b], Tayeb Chihi[c], and Messaoud Fatmi[d,]**

[a] *Department of Chemistry, Faculty of Technology, University of Mohamed Boudiaf, M'sila, 28000 Algeria*
[b] *Laboratory of Studies Surfaces and Interfaces of Solids Materials, Department of Physics, Faculty of Science, University Ferhat Abbas of Setif 1, Setif, 19000 Algeria*
[c] *Laboratory for Developing New Materials and their Characterization, Department of Physics, Faculty of Science, University of Setif 1, Setif, 19000 Algeria*
[d] *Research Unit on Emerging Materials (RUEM), University of Setif 1, Setif, 19000 Algeria*
** e-mail: Mohamedamine.ghebouli@univ-msila.dz*
*** e-mail: fatmimessaoud@yahoo.fr, med.amineghebouli@yahoo.fr*
Received October 29, 2020; revised October 29, 2020; accepted November 3, 2020

Abstract—We calculated equilibrium lattice constant a_0, bulk modulus B_0, pressure derivative B_0' and bond lengths $d_{F_i-F_j}$ and $d_{F_i-Sc_j}$ using both GGA and LDA approaches for ScF_3. We predict the elastic moduli using GGA and LDA functional. The ScF_3 is elastically and dynamically stable in the pressure range 0–38 GPa. The Young's modulus, shear modulus, linear compressibility and Poisson's ratio have a maximum value and another minimum in each direction explaining their anisotropy. The indirect R–X band gap value of 6.139 eV and the electronic DOS indicate the insulator character in ScF_3. The predicted GGA and LDA values of electron effective masses for ScF_3 are 1.604 and 1.703, respectively. The longitudinal and transversal optical phonon frequencies ω_{L0} and ω_{T0} at R point for ScF_3 are 725.69 and 588.5 cm^{-1}. The volumetric thermal expansion coefficient, the constant volume and pressure heat capacities and entropy at zero pressure and 300 K are 5.14×10^5 K^{-1}, 83.86, 86.54, and 77.48 J mol^{-1} K^{-1} for ScF_3. The edge of the optical absorption located at 31.53 nm is caused by V_1-C_1 transition at X point, which corresponds to the indirect band gap R–X.

Keywords: optical properties, bulk modulus, ScF_3
DOI: 10.1134/S0036024421150115

1. INTRODUCTION

Rare earth elements, lanthanides and scandium are very important in the field of electronic instruments. They are used in defense and in the energy and communication industry. Scandium fluoride ScF_3 belongs to a class of materials that show negative thermal expansion in the range 10–1100 K [1]. This material can take ReO_3 type cubic structure [2]. Sorokin et al. investigate experimentally the electrical ionic conductivity of ScF_3 for ReO_3 single crystal by using impedance spectroscopy [3]. Karimov et al. report that ScF_3 possess high thermal conductivity ($k = 9.6$ W m^{-1} K^{-1} at 300 K) and low ionic conductivity ($\sigma = 4 \times 10^{-8}$ S cm^{-1} at 673 K) [4]. Aleksandrov et al. studied the high-pressure phase of ScF_3 by using synchrotron radiation diffraction and Raman scattering [5]. ScF_3 was prepared by Newkirk [6] from a mixture of ScF_3 and NaF with a ratio of 20 : 80 and doped with 1% CrF_3. The detailed method of synthesis is explained in reference [6].

We use in this work the pseudo-potential plane-wave (PP-PW) method within the generalized gradient approximation (GGA) and local density approximation (LDA) to determine the structural, elastic, electronic, lattice dynamic, thermodynamic and optical properties of ScF_3 with a single cubic structure.

2. CALCULATION MODELS AND METHODOLOGY

The calculations were performed by using a pseudo-potential plane-waves (PP-PW) method of the density functional theory (DFT) as implemented in the CASTEP code [7]. The interactions of valence electrons with ion cores are treated in the reciprocal space with a Vanderbilt ultra soft pseudo potential [8]. We adopt the generalized gradient approximation

Table 1. The calculated equilibrium lattice constant a_0 (Å), bulk modulus B_0 (GPa), pressure derivative B_0', and bond lengths (Å) $d_{F_i-F_j}$ (Å) and $d_{F_i-Sc_j}$ (Å) using both GGA and LDA

Parameters		a_0	B_0	B_0'	d_{F1-F2}	d_{F1-F3}	d_{F2-F3}	d_{F1-Sc1}	d_{F2-Sc1}	d_{F3-Sc1}
This work	GGA	4.068	88.81 89.18	4.32 4.38	2.876	2.876	2.876	2.034	2.034	2.034
	LDA	3.978	106.06 105.45	4.32 4.27	2.813	2.813	2.813	1.989	1.989	1.989
Experiment		4.026 [18]	60 [19]		2.86 [21]	2.86 [21]	2.86 [21]	2.02 [21] 2.012 [6]	2.02 [21] 2.012 [6]	2.02 [21] 2.012 [6]
Other		4.074 [20] 3.986 [20]	89 [20] 106 [20]							

(GGA) of Perdew, Burke and Ernzerhof [9] and the local density approximation (LDA) with Teter and Pade parameterization [10] for the exchange-correlaion functional. The integration over the Brillouin zone is employed by using the Monkhorst-Pack method [11] with 8 × 8 × 8 k-points and cut-off energy of 360 eV. The optimization of the lattice constant corresponds to the minimum energy. The structural parameters were determined using the Broyden–Fletcher–Goldfarb–Shanno minimization technique [12]. The detailed study of thermal effect by using the quasi-harmonic Debye model implemented in the Gibbs program are found in [13–17].

3. RESULTS AND DISCUSSIONS

3.1. Structural Analysis

The scandium fluoride ScF_3 crystallizes in cubic structure with space group $Pm\bar{3}m$ (221). This structure shows that Sc and F atoms take positions 1*a* (0, 0, 0) and 3*d* (1/2, 0, 0). The equilibrium lattice constant a_0, bulk modulus B_0, the pressure derivative B_0' and bond lengths $d_{F_i-F_j}$ and $d_{F_i-Sc_j}$ are listed in Table 1 using both GGA and LDA approaches, along with the experimental [18, 19] and other theoretical values [20, 21] reported in the literature. The GGA parameters cited above at equilibrium are in well concordance with available experiment and other theoretical data. Note that the analysis of bond lengths indicates that $d_{F_i-F_j}$ distances are equal as well as$d_{F_i-Sc_j}$, but the later are smaller. We point out that our values agree well with the experiment ones quoted in references [6, 21].

3.2. Elastic Constants

The predicted elastic moduli at equilibrium and $\frac{\partial C_{11}}{\partial P}$, $\frac{\partial C_{12}}{\partial P}$, $\frac{\partial C_{44}}{\partial P}$, $\frac{\partial B}{\partial P}$ using GGA and LDA approaches for the scandium fluoride are reported in Table 2. For a cubic crystal under pressure, the generalized elastic stability criteria are [22]:

$$\begin{aligned} &C_{11} + 2C_{12} \succ 0, \quad C_{44} \succ 0, \\ &C_{11} - C_{12} \succ 0, \quad C_{12} \prec B \prec C_{11}. \end{aligned} \tag{1}$$

The calculated elastic moduli satisfy the above criteria at equilibrium, suggesting that ScF_3 is elastically stable. The bulk modulus, shear modulus, Young's modulus, Poisson's ratio and anisotropy factor deduced from Voigt [23], Reuss [24], and Hill [25] approximations are listed in Table 3. The Poisson's ratio of ScF_3 is around 0.25, and then this material has dominantly ionic bonding. The anisotropy factor value indicates a strong anisotropy in ScF_3. Figure 1 shows the direction-dependent Young's modulus, linear compressibility and Poisson's ratio for ScF_3. For the isotropic material, the shape is spherical and any distortion from the spherical shape indicates anisotropy. Consequently, Young's modulus, linear compressibility and Poisson's ratio for ScF_3 are anisotropic. The predicted maximum and minimum values for these parameters are listed in Table 4.

3.3. Electronic Properties

Figure 2a shows the plot of electronic band structure at equilibrium geometry along the high symmetry directions X, R, M, and Γ in the Brillouin zone using GGA approach. ScF_3 exhibits an indirect band gap R–X of 6.139 eV, which traduces its insulator character. For comparison, ScF_3 possesses an indirect band gap R–X of 5.947 eV [26]. We point out that the experimental band gap value for ScF_3 is located between 7–8 eV [27]. The upper valence band is located between −3.12 eV and the Fermi level. The first conduction band started at 6.18 eV above the Fermi level. We listed E_0, $\frac{\partial E}{\partial P}$, $\frac{\partial^2 E}{\partial P^2}$ for all band gaps with both GGA and LDA in Table 5. We also show the total and partial densities of states (TDOS and PDOS) of ScF_3 in

Table 2. The equilibrium elastic moduli (GPa), $\frac{\partial C_{11}}{\partial P}$, $\frac{\partial C_{12}}{\partial P}$, $\frac{\partial C_{44}}{\partial P}$, $\frac{\partial B}{\partial P}$ predicted using GGA and LDA for ScF_3

Parameters		C_{11}	C_{12}	C_{44}	B	$\frac{\partial C_{11}}{\partial P}$	$\frac{\partial C_{12}}{\partial P}$	$\frac{\partial C_{44}}{\partial P}$	$\frac{\partial B}{\partial P}$
This work	GGA	231.05	20.35	18.65	90.58	8.52	1.27	–0.57	4.20
	LDA	274.74	18.16	17.57	103.69	8.81	1.36	–0.55	4.09

Table 3. The bulk modulus, shear modulus, Young's modulus, Poisson's ratio and anisotropy factor for ScF_3

Parameters	B, GPa			G, GPa			E_H, GPa	σ_H	A_U
	B_V	B_R	B_H	G_V	G_R	G_H			
GGA	90.58	90.58	90.58	53.33	27.81	40.57	105.91	0.305	4.58
LDA	103.69	103.69	103.69	61.85	26.83	44.34	116.44	0.312	6.52

Fig. 2b. The upper valence band located in the range (−3.5 eV to E_F) is principally due to the F: *p* sites. The first conduction band located in the range 5.84 to 10.5 eV is mainly Sc: *d* states. We calculated the electron effective mass *m** in the conduction band minimum at the X valley in order to guarantee the parabolic shape by using the expression:

$$m^* = \pm\hbar^2\left(\frac{d^2E_k}{dk^2}\right)^{-1}. \quad (2)$$

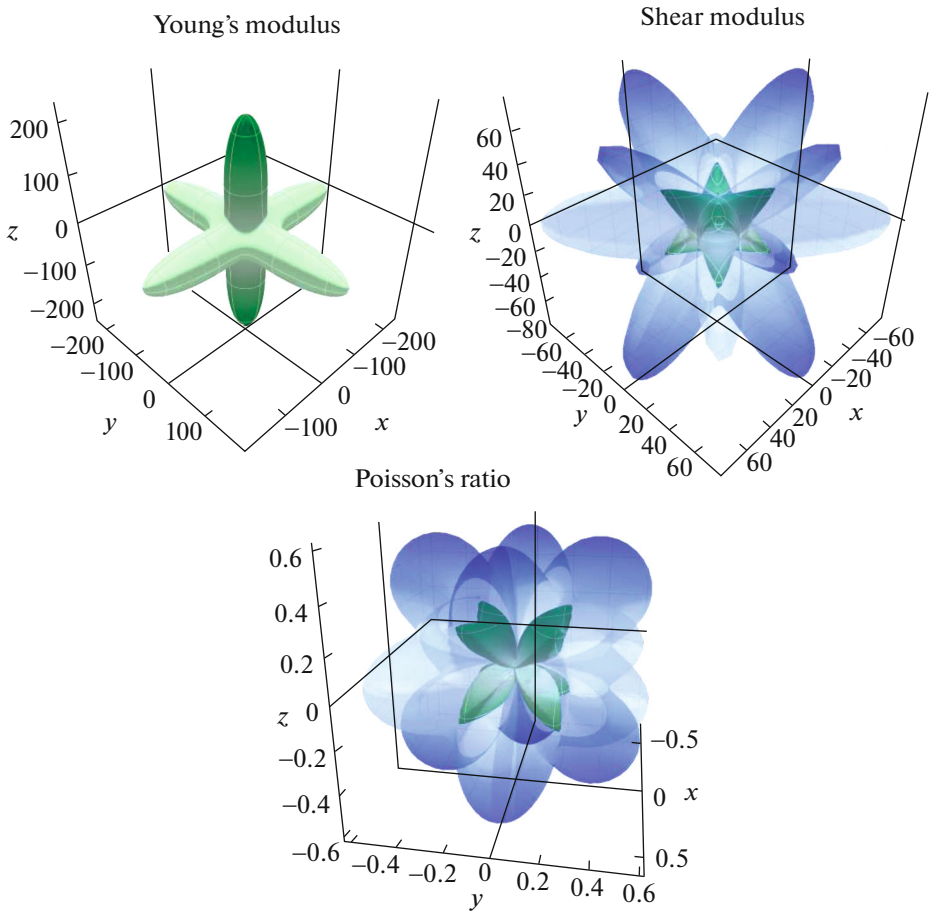

Fig. 1. The directional dependence of Young modulus, shear modulus, and Poisson ratio for ScF_3.

Table 4. The predicted direction-dependent Young's modulus, linear compressibility, shear modulus and Poisson's ratio for ScF_3

Parameters		Young's modulus, GPa		Linear compressibility		Shear modulus, GPa		Poisson's ratio	
		E_{min}	E_{max}	β_{min}	β_{max}	G_{min}	G_{max}	σ_{min}	σ_{max}
ScF_3	GGA	52.38	227.76	3.6796	3.6796	18.66	105.35	0.023	0.738
	LDA	49.90	272.49	3.2146	3.2146	17.57	128.29	0.014	0.784

Table 5. The $E_0, \frac{\partial E}{\partial P}, \frac{\partial^2 E}{\partial P^2}$ values for all band gaps calculated with both GGA and LDA for ScF_3

Parameters		E_{R-X}	E_{R-M}	$E_{R-\Gamma}$	E_{R-R}	E_{X-X}	$E_{\Gamma-\Gamma}$	E_{M-M}
LDA	E_0, eV	7.39	7.75	6.03	6.56	6.49	6.11	7.66
	$\frac{\partial^2 E}{\partial P^2}$ ($\times 10^{-4}$)	3.83	6.49	3.67	6.60	4.49	3.93	6.44
	$\frac{\partial E}{\partial P}$ ($\times 10^{-4}$)	−2.86	−4.49	−2.79	−4.09	−5.11	−4.53	−4.12
GGA	E_0, eV	7.27	7.58	6.13	6.69	6.65	6.17	7.27
	$\frac{\partial^2 E}{\partial P^2}$ ($\times 10^{-4}$)	−3.69	−5.14	−3.65	−5.02	4.90	−4.59	−5.15
	$\frac{\partial E}{\partial P}$ ($\times 10^{-4}$)	4.76	7.4	4.65	7.6	5.23	4.84	7.40

The GGA and LDA predicted values of electron effective masses for ScF_3 are 1.604 and 1.703, respectively.

3.4. Phonon Frequencies

We treat the lattice vibration in terms of the vibration norm-modes for acoustical or optical phonons frequencies and longitudinal or transversal propagation. We compute the phonons dispersions curves by using the density functional perturbation theory. Figure 3a shows the phonons dispersions curves and density of states of phonons for ScF_3. The unit cell of ScF_3 has four atoms and as a result there is optical branches and the remaining are acoustical. Our longitudinal and transversal optical phonons frequencies ω_{L0} and ω_{T0} at R point for ScF_3 are 725.69 and 588.5 cm^{-1}. There are no soft modes, and consequently this material is dynamically stable. We point out that the main features of phonons dispersions spectra are the followings.

(1) The longitudinal optical (LO) and transversal optical (TO) branches are separated by a frequency gap of 67 cm^{-1}.

(2) There is a frequency gap of 116 cm^{-1} between optical and acoustical modes.

(3) F atoms and small contribution of Sc atoms are responsible to the optical and acoustical modes.

(4) The maximum of longitudinal and transversal optical branches are located at the R point.

(5) There is an overlapping between longitudinal and transversal acoustical branches.

Figure 3b represents the phonons dispersions curves of ScF_3 at 40 GPa. We see that beyond 38 GPa, ScF_3 becomes dynamically unstable.

3.5. Thermodynamic Properties

We investigate the thermodynamic properties of ScF_3 under high temperature in the range from 0 to 1800 K and pressure from 0 to 50 GPa. Figure 4a presents the volume–temperature diagram of ScF_3 at several pressures. The volume increases with increasing temperature at a given pressure. On the other side, as the pressure increases the volume decreases at a given temperature. At 300 K and zero pressure, the lattice constant is 4.0768 Å. Figure 4b shows the bulk modulus versus temperature at a given pressure. The bulk modulus decreases with increasing temperature at a given pressure and increases with increasing pressure at a given temperature. At 300 K and zero pressure, the bulk modulus is 85.62 GPa. Figure 4c displays the dependence of the Debye temperature θ_D on temperature and pressure. The Debye temperature is practically constant between 0 and 300 K, and then it decreases linearly with increasing temperature. It is

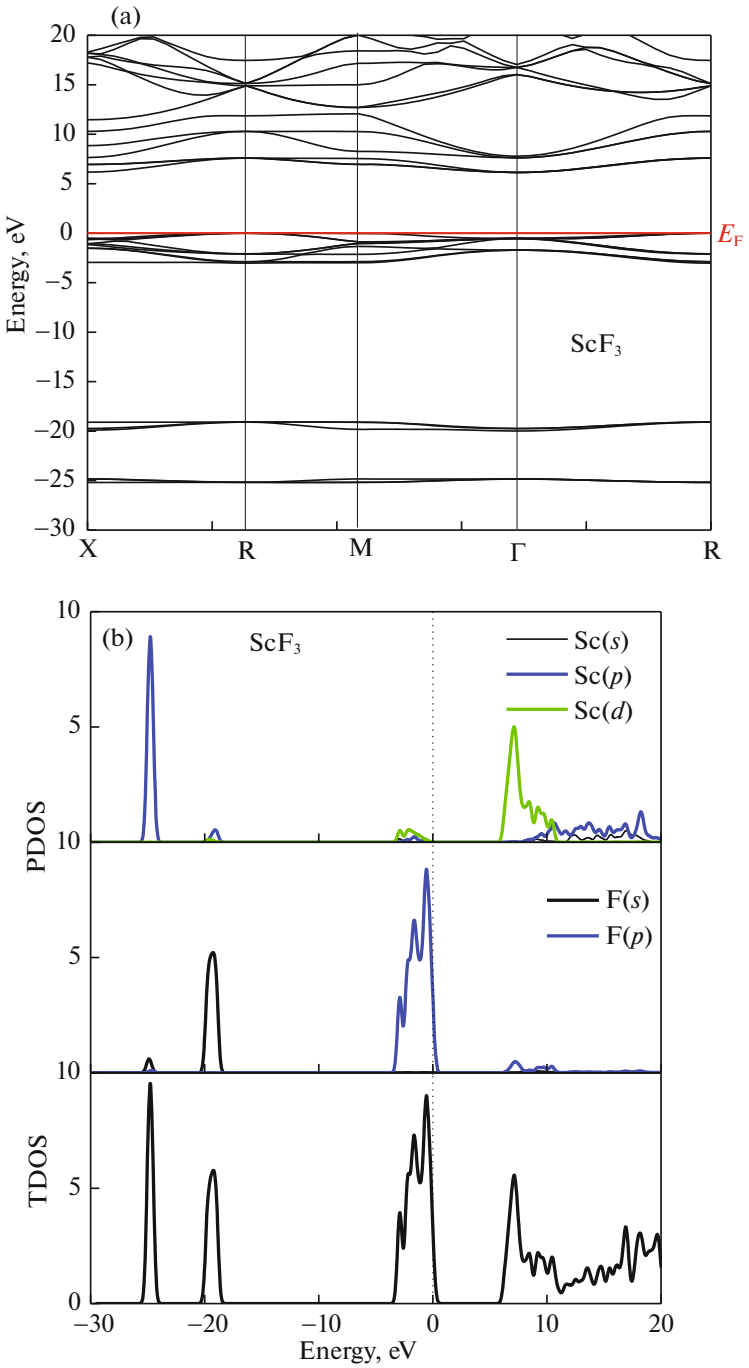

Fig. 2. The band structure along the high symmetry points X, R, M and Γ (a), total and partial densities of states (b) for ScF_3.

also shown that when the temperature is constant, the Debye temperature increases almost with applied pressure. Our calculated θ_D at zero pressure and 300 K is 467.18 K, which is in reasonable agreement with the value computed accurately in terms of the elastic constants 476 K. Figure 5a plots the volumetric thermal expansion coefficient α as a function of temperature and pressure. It is shown that, at a given pressure, α increases sharply with the increase of temperature up to 300 K. When $T > 300$ K, α gradually approaches to a linear increase with increase in temperature, and the propensity of increment becomes moderate, which means that the temperature dependence of α is very small at high temperature. For a given temperature, α decreases drastically with the increase of pressure. At 300 K and zero pressure, α is 5.14×10^5 K^{-1}.

Figures 5b and 5c represent the constant volume and pressure heat capacities C_V and C_P as a function of

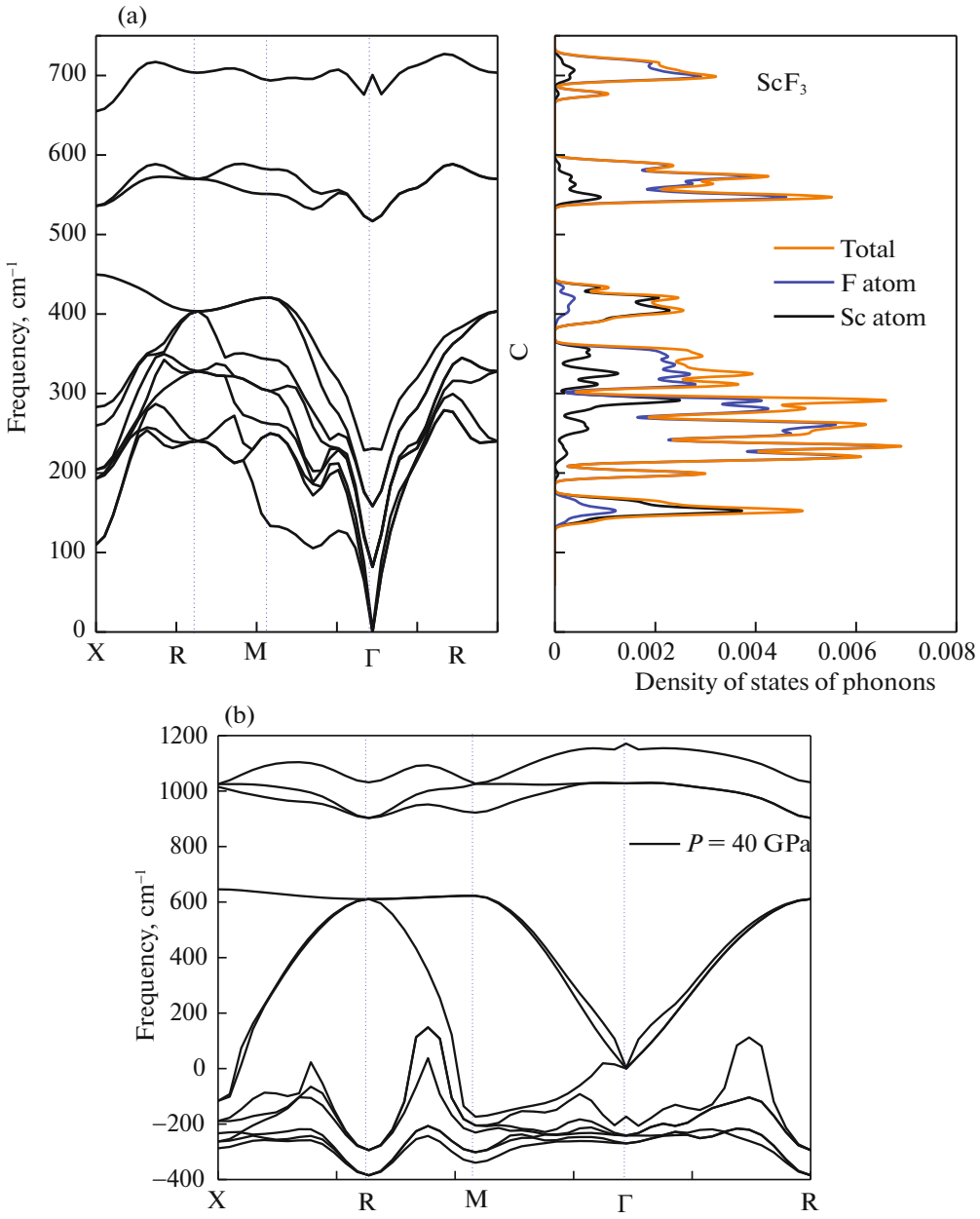

Fig. 3. Phonons dispersions curves and density of states of phonons for ScF_3 (a) at equilibrium pressure (b) at pressure of 40 GPa.

the temperature. At sufficiently low temperature, C_V is proportional to T^3 [28]. Then up to 450 K, C_V and C_P increase exponentially and the difference between them is very slight. At high temperature ($T > 450$ K) C_P follows a linear increase, whereas C_V tends to the Petit and Dulong limit [29], which is common to all solids at high temperature. At high temperature C_V tends to approach 98.1 J mol^{-1} K^{-1}. At zero pressure and ambient temperature, C_V and C_P are 83.36 J mol^{-1} K^{-1} and 86.54 mol^{-1} K^{-1}, respectively. The constant pressure heat capacity and entropy predicted using GGA along with experimental values for ScF_3 are listed in Table 6.

3.6. Optical Properties

Figure 6a displays the plot of imaginary part of the dielectric function (right panel) and the transition energy $E(k) = E_{Cj}(k) - E_{Vi}(k)$ (left panel), where V_i and C_j are the valence band number i and the conduction band number j. The main optical transitions are described from the upper five valence bands to the five low conduction bands. All possible transitions are reported in Table 7. Figure 6b displays the optical constants as a function of wavelength for ScF_3. The edge of the optical absorption located at 31.53 nm is caused by V_1–C_1 at R point in Brillouin zone, which corre-

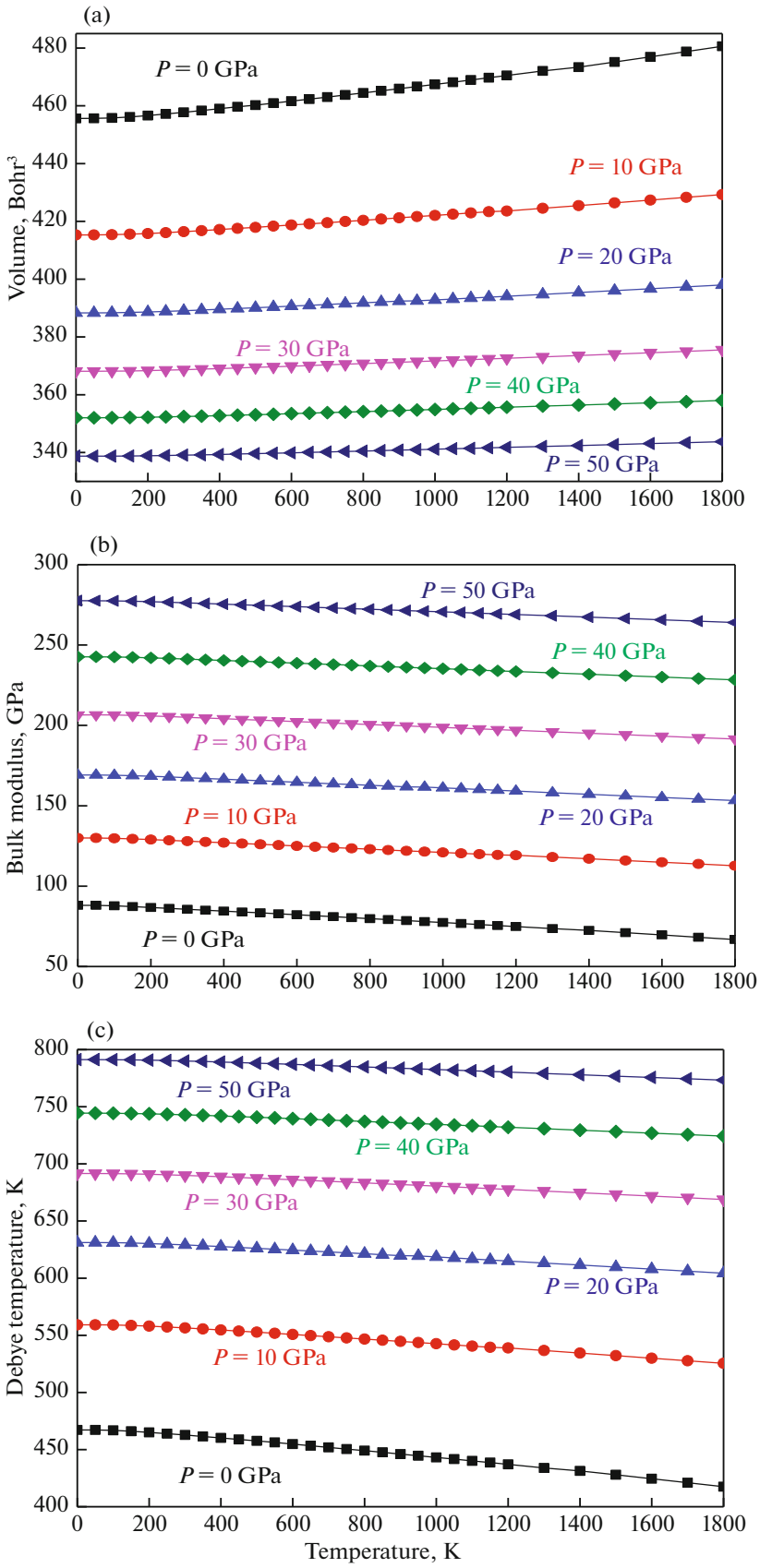

Fig. 4. Volume (a), bulk modulus (b), and Debye temperature (c) as a function of temperature for ScF_3.

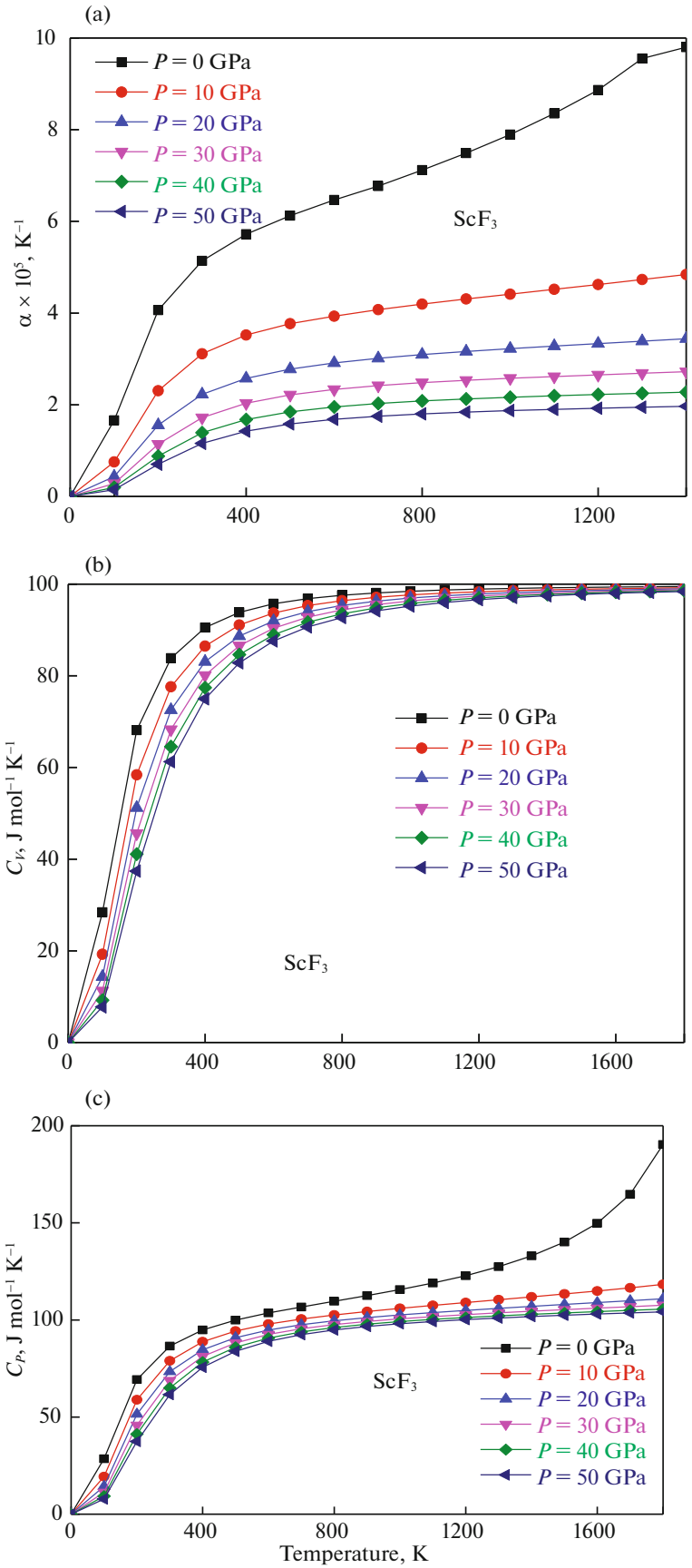

Fig. 5. Volumetric thermal expansion coefficient (a), constant volume (b), and pressure (c) heat capacities versus temperature for ScF_3.

Table 6. The constant pressure heat capacity and entropy (calculated using GGA and experimental values) for ScF_3

Temperature, K	C_P, J mol^{-1} K^{-1}		S, J mol^{-1} K^{-1}	
	this work	experiment [21]	this work	experiment
0	0		0	
100	28.508		11.549	
200	69.305		45.618	
300	86.546	83.881	77.482	97.907
400	94.870	91.046	103.649	101.302
500	99.914	94.357	125.397	144.408
600	103.606		143.952	161.839
700	106.673	97.943	160.039	176.835
800	109.609	98.94	174.558	189.982
900	112.548	99.727	187.679	201.682
1000	115.633		199.698	212.224
1100	119.022		210.873	221.819
1200	122.773		221.271	230.625
1300	127.413		231.388	238.765
1400	132.991		241.044	246.335
1500	140.124		250.452	253.412
1600	149.763		259.735	260.059
1700	164.717		269.285	266.328
1800	190.341		279.127	272.257

sponds to the indirect band gap R–X. The maximum reflectivity value is 338468 cm^{-1} at 38.26 nm. The peaks of energy loss correspond to the trailing edges in the reflection spectra. The prominent peaks of loss are situated at energies corresponding to the abrupt reductions of reflectivity. The loss function reached a maximum value of 1.49 at 37 nm for ScF_3. We observed that the reflectivity of ScF_3 has a value of 0.003, which corresponds to a wavelength of 30.44 nm. After a successive growth it reached a maximum value of 0.17 at 123.9 nm. It is reported in a number of previous investigations that the lower reflectivity indicates the higher UV or visible light absorption [21]. These absorption peaks are attributed to the photo transition energies from the maximum valence band to the minimum conduction band under UV light irradiation, which indicates that this material can absorb photons of UV range. The highest value of absorption 338468 cm^{-1} was determined at the wavelength of 38.26 nm. One can see that maximum of absorption corresponds to the maximum of reflectivity and the no loss function.

4. CONCLUSIONS

We obtain the structural, elastic, electronic, lattice dynamic, thermodynamic and optical properties of cubic ScF_3 by using the pseudo-potential plane-wave (PP-PW) method within the generalized gradient approximation (GGA) and local density approximation (LDA). The computed value of the factor anisotropy and Poisson's ratio indicate that ScF_3 has a strong anisotropy and predominantly ionic bonding. The optical properties of ScF_3 such as all possible transitions, absorption, reflectivity and loss function were investigated. F atoms and small contribution of Sc atoms contribute to the optical and acoustical modes, where there is a gap of 67 cm^{-1} between them. The unit cell volume increases with increasing temperature at a given pressure and decreases when the pressure is increased at a given temperature. The predicted Debye temperature at zero pressure and 300 K is 467.18 K, which is in reasonable agreement with the value computed accurately with elastic constants (476 K). The upper valence band located in the range (–3.5 eV to

Table 7. The main contribution to the optical transitions from the top five valence bands to the lower five conduction bands for ScF_3

Brillouin zone	$X \to R$	$M \to \Gamma$	$\Gamma \to R$
$E = 7.23$ eV	$V_5 \to C_1, V_4 \to C_1, V_3 \to C_1, V_2 \to C_1, V_1 \to C_1$	$V_1 \to C_3, V_2 \to C_1, V_2 \to C_3, V_2 \to C_2, V_4 \to C_1, V_4 \to C_2, V_3 \to C_2, V_5 \to C_1, V_5 \to C_2$	$V_1 \to C_3, V_3 \to C_1, V_3 \to C_3, V_5 \to C_1, V_5 \to C_3$
$E = 9.60$ eV	$V_3 \to C_5, V_6 \to C_3, V_4 \to C_4, V_5 \to C_3, V_5 \to C_1, V_2 \to C_5, V_5 \to C_4, V_4 \to C_1, V_4 \to C_2, V_5 \to C_2$	$V_6 \to C_3, V_6 \to C_4, V_6 \to C_6, V_6 \to C_5, V_5 \to C_6, V_3 \to C_6, V_5 \to C_3$	$V_6 \to C_6, V_5 \to C_6, V_3 \to C_6, V_1 \to C_6, V_3 \to C_6, V_1 \to C_4$
$E = 13.28$ eV	$V_6 \to C_3, V_5 \to C_7, V_4 \to C_7, V_6 \to C_6, V_5 \to C_6, V_5 \to C_6, V_4 \to C_6, V_1 \to C_7$	$V_6 \to C_6, V_1 \to C_7, V_5 \to C_6, V_3 \to C_6$	$V_5 \to C_6, V_6 \to C_6, V_3 \to C_7, V_1 \to C_7$
$E = 16.01$ eV	$V_6 \to C_7, V_5 \to C_7$	$V_6 \to C_7, V_2 \to C_7, V_5 \to C_7, V_1 \to C_7$	$V_5 \to C_7, V_3 \to C_7, V_1 \to C_7$

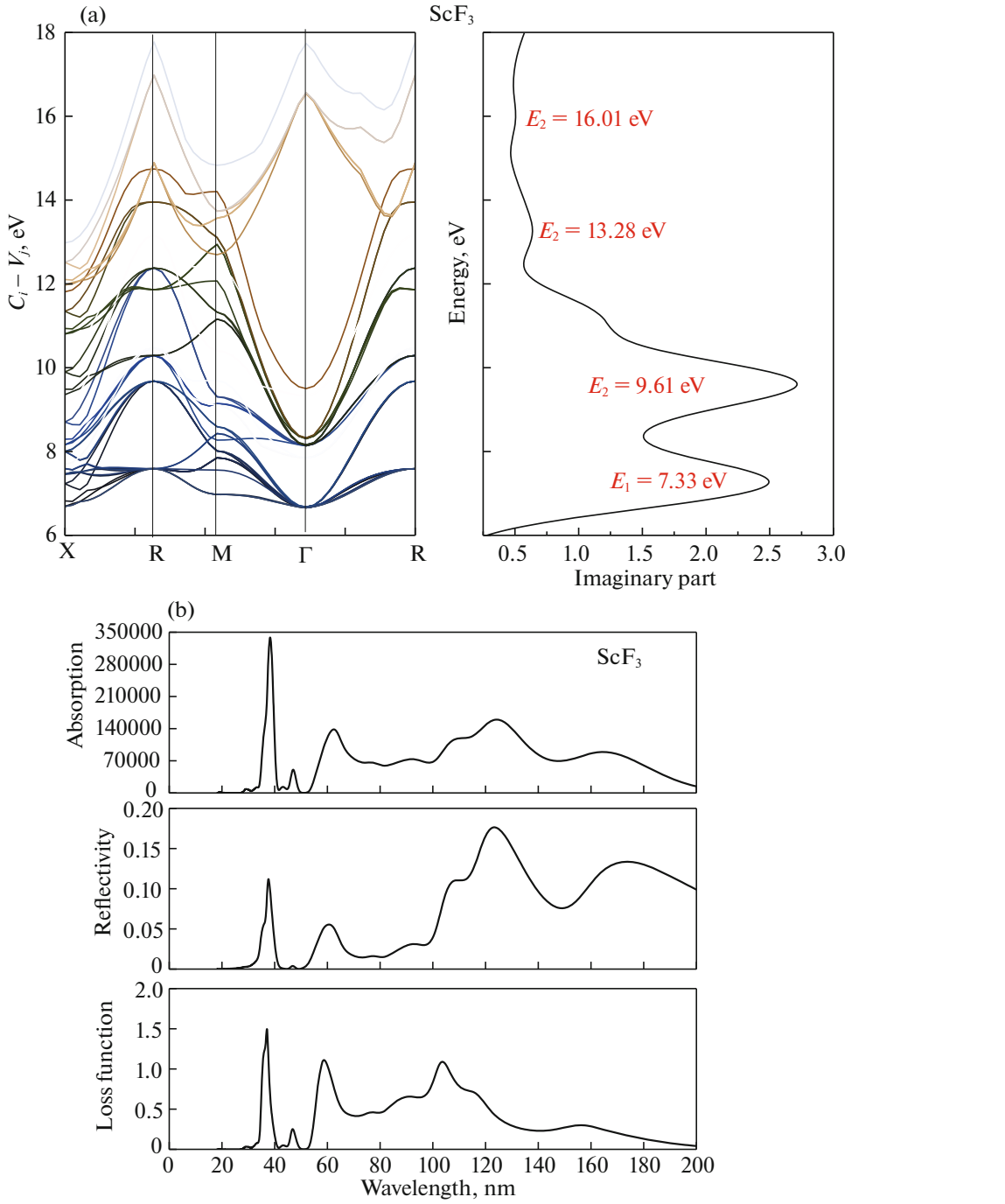

Fig. 6. Optical transitions energies $E(k) = E_{Cj}(k) - E_{Vi}(k)$ (left panel), imaginary part (right panel) (a) and optical constants (b) for ScF_3.

E_F) is principally due to the F: *p* sites. The first conduction band located in the range 5.84 to 10.5 eV is mainly Sc: *d* states.

REFERENCES

1. G. Kresse and J. Furthmüller, *VASP the Guide* (Inst. Materialphysik, Univ. Wien, Wien, Austria, 2007).
2. L. Wang, C. Wang, Y. Sun, K. Shi, S. Deng, H. Lu, P. Hu, and X. Zhang, J. Materiomics **1**, 106 (2015).
3. N. I. Sorokin, D. N. Karimov, V. V. Grebenev, and B. P. Sobolev, Crystallogr. Rep. **61**, 270 (2016).
4. D. Karimov, I. Buchinskaya, N. Arkharova, P. Prosekov, V. Grebenev, N. Sorokin, T. Glushkova, and P. Popov, Crystals **9**, 371 (2019). https://doi.org/10.3390/cryst9070371

5. K. S. Aleksandrov, N. V. Voronov, A. N. Vtyurin, A. S. Krylov, M. S. Molokeev, A. S. Oreshonkov, S. V. Goryainov, A. Yu. Likhacheva, and A. I. Ancharov, Phys. Solid State **53**, 564 (2011).
6. G. Huber, S. A. Payne, L. L. Chase, and W. F. Krupke, J. Lumin. **39**, 259 (1988).
7. S. J. Clark, M. D. Segall, C. J. Pickard, P. J. Hasnip, M. J. Probert, K. Refson, and M. C. Payne, Zeitschr. Kristallogr. **220**, 567 (2005).
8. D. Vanderbilt, Phys. Rev. B **41**, 7892 (1990).
9. J. P. Perdew, K. Burke, and M. Ernzerhof, Phys. Rev. Lett. **77**, 3865 (1996).
10. S. Goedecker, M. Teter, and J. Hutter, Phys. Rev. B **54**, 1703 (1996).
11. H. J. Monkhorst and J. D. Pack, Phys. Rev. B **13**, 5188 (1976).
12. T. H. Fischer and J. Almlof, J. Phys. Chem. **96**, 9768 (1992).
13. M. A. Blanco, E. Francisco, and V. Luaña, Comput. Phys. Commun. **158**, 57 (2004).
14. M. A. Blanco, A. M. Pendás, E. Francisco, J. M. Recio, and R. Franco, J. Mol. Struct.: THEOCHEM **368**, 245 (1996).
15. M. Flórez, J. M. Recio, E. Francisco, M. A. Blanco, and A. M. Pendás, Phys. Rev. B **66**, 144112 (2002).
16. E. Francisco, J. M. Recio, M. A. Blanco, and A. M. Pendás, J. Phys. Chem. **102**, 1595 (1998).
17. E. Francisco, M. A. Blanco, and G. Sanjurjo, Phys. Rev. B **63**, 049107 (2001).
18. B. K. Greve, K. L. Martin, P. L. Lee, P. J. Chupas, K. W. Chapman, and A. P. Wilkinson, J. Am. Chem. Soc. **132**, 15496 (2010).
19. C. R. Morelock, B. K. Greve, L. C. Gallington, K. W. Chapman, and A. P. Wilkinson, J. Appl. Phys. **114**, 213501 (2013).
20. Y. Oba, T. Tadano, R. Akashi, and Sh. Tsuneyuki, Phys. Rev. Mater. **3**, 033601 (2019).
21. K. H. Jack and V. Gutman, Acta Crystallogr. **4**, 246 (1951).
22. G. V. Sin'ko and N. A. Smirnov, J. Phys.: Condens. Matter **14**, 6989 (2002).
23. W. Voigt, *Lehrbuch der Kristallphysik* (Vieweg +Teubner Verlag, Wiesbaden, 1966).
24. A. Reuss, Zeitschr. Angew. Math. Mech. **9**, 49e58 (1929).
25. R. Hill, Proc. Phys. Soc. **65**, 349e54 (1952).
26. Rui Zhu, Yushun Zeng, Shanchuan Liang, Yu Zhang, Yunhui Qi, Yunfei Liu, and Yinong Lyu, J. Solid State Chem. **269**, 447–453 (2019). https://doi.org/10.1016/j.jssc.2018.10.015
27. M. Umeda, Y. Tezuka, S. Shin, and A. Yagishita, Phys. Rev. B **53**, 1783 (1996).
28. P. Debye, Ann. Phys. **39**, 789 (1912).
29. A. T. Petit and P. L. Dulong, Ann. Chim. Phys. **10**, 395 (1819).